AIMS Materials Science, 9(3): 344–358.
DOI: 10.3934/matersci.2022021
Received: 25 October 2021
Revised: 05 February 2022
Accepted: 13 March 2022
Published: 30 March 2022

http://www.aimspress.com/journal/Materials

Research article

Composite scaffolds of chitosan/polycaprolactone functionalized with protein of *Mytilus californiensis* for bone tissue regeneration

Miguel-Angel Rojas-Yañez[1], Claudia-Alejandra Rodríguez-González[1], Santos-Adriana Martel-Estrada[2], Laura-Elizabeth Valencia-Gómez[1], Claudia-Lucia Vargas-Requena[3], Juan-Francisco Hernández-Paz[1], María-Concepción Chavarría-Gaytán[1] and Imelda Olivas-Armendáriz[1,*]

[1] Institute of Engineering and Technology, Autonomous University of Ciudad Juarez, Ciudad Juárez, Chihuahua, México, Mexico
[2] Institute of Architecture Design and Art ffiliation, Autonomous University of Ciudad Juarez, Ciudad Juárez, Chihuahua, México, Mexico
[3] Institute of Biomedical Sciences, University of Ciudad Juarez, Ciudad Juárez, Chihuahua, Mexico

* **Correspondence:** Email: iolivas@uacj.mx; Tel: +52-656-176-1524.

Abstract: Nowadays, the treatment for bone damage remains a significant challenge. As a result, the development of bioactive three-dimensional scaffolds for bone regeneration has become a key area of study within tissue engineering. This research is focused on the evaluation of the properties of Chitosan (Ch)/Polycaprolactone (PCL) scaffolds with the *Mytilus californiensis* protein by Thermally Induced Phase Separation (TIPS). This study used the extrapalleal fluid protein from *Mytilus californiensis* because it increases biological processes that support bone regeneration. Two methodologies were used for the scaffolds functionalization: (I) an immersion process in a solution with the protein and (II) the protein direct addition during the scaffold synthesis. The scaffolds were analyzed by Fourier Transformed Infrared Spectroscopy (FT-IR), Scanning Electron Microscopy (SEM), and Mechanical Compression test to determine the composition, morphology, and mechanical properties of each material. *In vitro* analysis of biodegradation, bioactivity, and biocompatibility were also performed. The scaffolds with the protein added directly presented superior properties in the tests of bioactivity and cellular proliferation, making these composites attractive for the area of bone regeneration.

Keywords: polymer composites; polycaprolactone; chitosan; *Mytilus californiensis*; biocompatible polymers

1. Introduction

Bone regeneration is a health issue mainly due to traffic accidents, injuries, burns, among other [1]. Nevertheless, reconstruction of the damaged bone remains clinically challenging in medicine [2,3]. Scaffolds are a proposed solution to promote new bone formation, and to regulate the proliferation and differentiation of cells. The ideal bone tissue engineering scaffolds must have the appropriate porosity, mechanical support, biocompatibility, surface activity, and shape to promote cell adhesion [1,4].

The current trend in bone tissue engineering is the use of bioactive materials capable of specific biological processes for a faster and safer bone tissue regeneration. This trend has generated the need to functionalize polymeric biomaterials with biomolecules that induce the desired biological processes [2–4]. The use of proteins, enzymes, and other types of nutrients is an alternative to make bone regeneration processes more efficient. Some studies regarding the biomineralizing activity of proteins and its effect on scaffolds for bone tissue regeneration have shown that protein from mollusks such as pearl oyster promote higher organization of the inorganic crystals in the collagen fibers of the matrix [5]. Other studies have shown similar mechanisms, where the presence of bioproteins from mollusks have been related to osteoprogenitor properties [3]. These biomolecules have also assisted in nucleation and have provided order that benefits biomineralization [4].

Various natural and synthetic polymers have played an important role in the development of scaffolds that can help in the bone regeneration process [4–5] since polymers have similar structure and properties to that of natural extracellular matrix [6–10]. Chitosan (Ch) is a biomaterial used in the food industry, agriculture, drugs, cosmetology, and textile industry. It is derived from chitin's deacetylation, and it is the second most abundant polymer [11]. It is biocompatible, non-toxic, and biodegradable [12]. Also, it has antibacterial activity against fungi, gram-positive and gram-negative bacteria [13]. On the other hand, polycaprolactone (PCL) is a low-cost polymer, biodegradable, biocompatible semicrystalline, and aliphatic polyester with modulated mechanical and physical properties [9,14]. It has been used as a suture material, drug delivery system, and sensor in the biomedical field [15]. This substance is semicrystalline at room temperature, and the melting temperature is around 60 ℃ [16].

Mytilus californiensis is a glycoprotein that has been studied due to its biomineralization-promoting properties. This is a mollusk whose fluid located between its epithelial mantle and its shell are concentrated substances such as K^+, Ca^+, Mg^+, H_2CO_3, Cl^- and Na^+ that favor the biomineralization process [17].

According to the characteristics described above, it is possible to consider that a material composed of chitosan/polycaprolactone will have the appropriate attributes to be used as a matrix for bone regeneration. At the same time, the protein of *Mytilus californiensis* will contribute to improve its bioactivity. However, to the best of our knowledge, the effect of this protein in scaffolds has not been reported up to date. For all the above, this research work evaluates the effects of the protein of

Mytilus californiensis on the properties of a scaffold made from Ch and PCL.

2. Materials and methods

2.1. Obtaining extrapallial fluid of Mytilus californiensis (EP)

The EP was obtained according to the methodology of Jaramillo-Martinez and collaborators [17]. The organisms were obtained from Baja California, Mexico, for EP release it was subjected to thermal stress, temperatures of 4 and 20 ℃ were applied at intervals of 4 h and 30 min, respectively. The EP was centrifuged, and the obtained supernatant was dialyzed at room temperature. The dialyzed sample was centrifuged again, and the supernatant was concentrated to 2.6 mg/mL. Subsequently, it was filtered and passed, at a flow of 1 mL/min, through a column with anion exchange matrix (Aligent BioWax NP 5, 4.6 × 250 mm) previously equilibrated with MOPS-NaCl buffer, in a high-resolution system. The fractions were eluted and analyzed by 15% SDS-PAGE and the molecular weight marker was used as a reference for migration.

2.2. Scaffolds synthesis

Ch (minimum 85% deacetylated, SIGMA) and PCL (average Mn 80000, SIGMA) were dissolved separately, PCL in a solution of 2.5 mL of glacial acetic acid (J. T. Baker) at 50% by magnetic stirring at 40 ℃. The solution was neutralized with a sodium hydroxide solution. On the other hand, Ch was dissolved in a 1% acetic acid solution at room temperature. Once both solutions were homogenized, the PCL solution was poured drop by drop into Ch solution at constant stirring. The obtained mixture was frozen at −80 ℃ for 2 h. After the freezing time, the sample was lyophilized for 72 h. Finally, the samples were neutralized with two 12 h immersions in 97% ethanol at −20 ℃ and 5 washes with distilled water. A 70/30 PCL/Ch scaffold (w/w) was obtained. The protein addition was performed in two ways; the first was by adsorption, leaving the material immersed in a protein-rich solution, which was identified as PCL/Ch/EPI. The second is by directly adding the protein to the solution where the polymeric matrix was synthesized (PCL/Ch/EPM). In both methodologies, the added protein was 1% concerning the weight of the synthesized material.

2.3. Chemical characterization

Fourier transform-infrared (FT-IR) spectroscopy was used to identify the functional groups in the composition of the scaffolds. The analysis was performed in a frequency range of 4000–500 cm^{-1} using FT-IR spectrophotometer (Nicolet model 6700). The scaffolds were cut and mounted in a glass adapter with Germanium STR for analysis.

2.4. Microstructure and porosity

The microstructure and porosity were characterized by a Field Emission SEM JEOL JSM-7000F. The electron beam accelerating voltage was 15 kV. Porosity diameter average was measured using

the ImageJ software analysis.

2.5. Mechanical characterization

The mechanical properties of the scaffolds were evaluated under compression at room temperature in a universal tensile testing machine (Tinius Olsen, HSOKS) and tested at a speed of 5 mm/min, 500 N loading cell, five repetitions of each condition were performed.

2.6. Enzymatic degradation in vitro

Samples of 1.0 × 1.0 cm were weighed and exposed to a 1X phosphate buffer solution (PBS) (pH 7.4) containing 0.02% sodium azide (≥99%, ultra-dry, Sigma-Aldrich) and 5 µg/mL lysozyme enzyme (protein ≥90%, Sigma Aldrich). They were incubated at 37 ℃ for 7, 14, and 21 d. After the incubation time was completed, the samples were removed from the PBS solution and washed with distilled water, dried in an oven under vacuum at room temperature, and weighed again. The remaining weight of the composite scaffolds was determined.

2.7. Bioactivity study

The bioactivity *in vitro* of the scaffolds was obtained using a solution of 1.5 × of Simulated Body Fluid (SBF). All samples of approximately 1.0 × 1.0 × 1.0 cm were immersed in the 1.5 × SBF solution with pH 7.4 at 37 ℃ for 7, 14, and 21 d. After each incubation period, three samples were removed from the SBF solution and washed with distilled water, and freeze-dried. All samples were characterized to evaluate the apatite forming ability using a scanning electron microscope (SEM), energy dispersive X-ray spectroscopy (EDS), X-ray diffraction analysis (XRD), and Fourier transform infrared (FT-IR) spectrometer techniques.

2.8. Cytotoxicity analysis

The cytotoxicity of the scaffolds was evaluated using an MTT assay (3-[4, 5-dimethlythiazol-2-yl]-2, 5-diphenyl tetrazolium bromide). All scaffolds were exposed to UV for sterilized and placed in 12 well plates. 5000 osteoblasts cells were seeded onto the scaffold and allowed to adhere and proliferate in a 5% CO_2 incubator at 37 ℃. Cells without samples were used as negative controls. After 7 and 14 d of incubation, the osteoblasts were treated with a MTT solution (0.5 mg/mL) and incubated at 37 ℃ for 3 h. The formazan complex formed during the incubation time was dissolved using DMSO (dimethyl sulphoxide). The absorption of the obtained solutions was measured at 570 nm in a microplate reader (Benchmark Plus).

2.8.1. Alkaline phosphatase activity

Composite scaffolds with 5000 osteoblasts cells were used for an Alkaline phosphatase (ALP) activity analysis at 7 and 14 d. After each incubation time osteoblasts cultured were lysed with 1%

Triton X-100 in DEPC-treated water and three freeze-thaw cycles. A volume of the sample was added to 100 μL of the p-nitrophenyl phosphate solution (PIERCE biotechnology, Monterrey, México) and incubated at room temperature for 30 min and then the reaction was stopped by the addition of 50 μL of 2 N·NaOH. The production of p-nitrophenol was determined by the absorbance at 405 nm.

2.8.2. Immunofluorescent imaging of cell markers: cell adhesion

The cell morphology analysis of viable cells was done in samples dyed with the fluorophores DAPI and calcein-AM (Invitrogen™, Thermo Fisher Scientific, Waltham, MA, USA). After 7 d of cultured, the culture medium was removed and substituted with 60 μL of each of the freshly prepared solutions (10 μg of DAPI in 100 mL of PBS, and 50 μg of calcein-AM in 10 mL of PBS) and 150 μL of new culture medium. Then, the solutions were allowed to incubate for 45 min and then observed using fluorescence microscopy (Axio Vert. A1, Carl Zeiss), and the ZEN blue software to capture the images.

2.9. Statistical analysis

All the experimental studies were carried out three times and the results were expressed as mean and standard deviation from the replicate values. The statistical analysis was performed using the student's T-test. $P \leq 0.05$ was considered statistically significant.

3. Results and discussion

3.1. Chemical and structural composition of scaffolds

The functional groups of the scaffolds were studied using FT-IR analysis as shown in Figure 1. The bands at 2944 and 2864 cm^{-1} were attributed to the asymmetric and symmetric stretching of the CH_2 group. The band with the highest intensity at 1723 cm^{-1} corresponds to the stretching vibrations of the carbonyl group C = O. This band shows interaction by hydrogen bonding with the chitosan chain [18]. Another band at 1293 cm^{-1} is assigned to the main chain C–C. At 1242 and 1188 cm^{-1}, there are bands assigned to asymmetric and stretching modes of the C–O–C group [19]. The bands at 1723, 1560, 1410, and 1322 cm^{-1} are assigned to stretching vibrations of the carbonyl group (amide I), to the deformation of the NH (amide II), flexion vibration of the CH, and stretching vibrations of the chitosan C–N (amide III). A band at 1080 cm^{-1} is due to vibration of stretching of the C–O bond [20]. These monomeric units of the protein can be identified through the bands located between the wavenumbers 640–800 cm^{-1} and the band at 3300 cm^{-1} where the resonance of the N–H bond occurs, while in the band between 1480, and 1575 cm^{-1} the N–H bond is expressed.

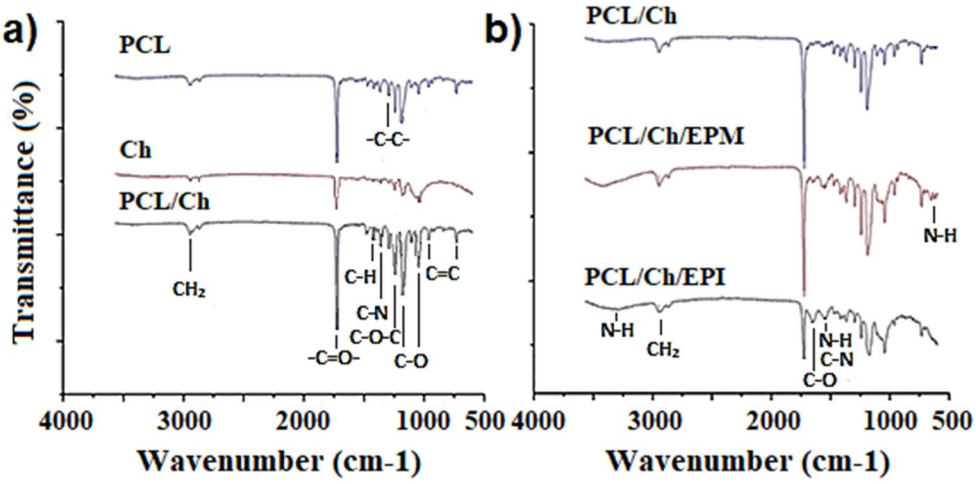

Figure 1. (a) PCL, Ch, and PCL/Ch spectra. (b) PCL/Ch, PCL/Ch/EPM, and PCL/Ch/EPI spectra.

According to the FTIR analysis, the union with the main chain polymers can be observed in the band between 1480 and 1575 cm^{-1} expressed by the stretching of the C–N. On the other hand, the carboxyl group present in the protein structure is detected in the bands between 1610 and 1695 cm^{-1} (stretching of the C–O junction) [21]. These results are in agreement with previous research, which found evidence of hydrogen bonding between the carbonyl group of PCL and the hydroxyl or amine group of chitosan [22].

Cross-sectional SEM micrographs of the scaffolds are shown in Figure 2. Porosity and interconnected structures are observed. The PCL/Ch/ EPM scaffold has the lowest average pore size, as shown in Table 1 where the average pore diameter sizes were 132.92, 136.32 and, 108.07 μm for the PCL/Ch, PCL/Ch/EPI, and PCL/Ch/EPM scaffolds, respectively.

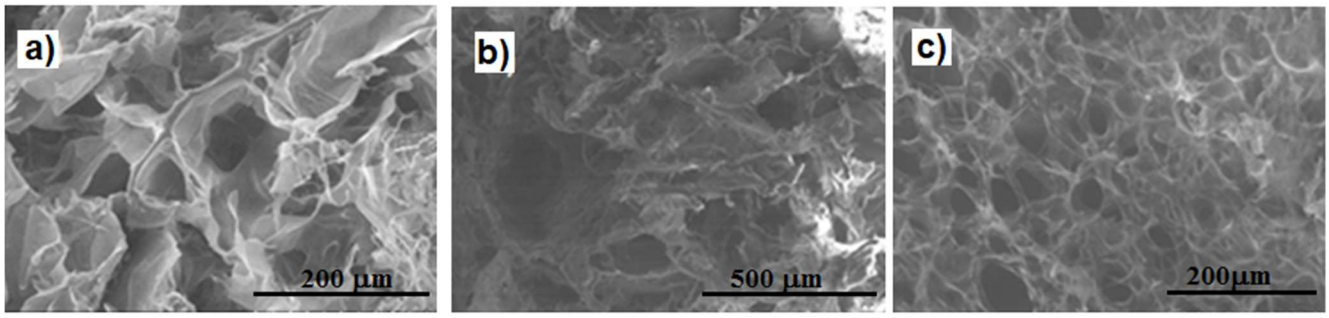

Figure 2. SEM images of the materials (a) PCL/Ch (b) PCI/Ch/EPI (c) PCL/Ch/EPM.

Table 1. The average pore size (μm) and pore size distribution (%) in PCL/Ch, PCL/Ch/EPI, and PCL/Ch/EPM scaffolds.

Sample	Average pore size (μm)	<50 μm	50–100 μm	100–150 μm	150–200 μm	>200 μm
PCL/Ch	132.92 ± 96.0	19.0%	12.0%	48.0%	11.0%	10.0%
PCL/Ch/EPI	136.32 ± 70.4	18.0%	23.0%	40.0%	12.0%	6.0%
PCL/Ch/EPM	108.07 ± 32.6	10.0%	39.0%	46.0%	4.0%	1.0%

The observed pore sizes suggest a possible dependence of the size on the protein integration method in the polymeric matrix. Results that according to Jaramillo-Martínez et al. can be attributed to the interaction of hydrogen bonds and Van der Waals forces between the protein (basic aminoacids and acidic aminoacids) and the polymeric matrix (carboxyl and hydroxyl groups) [17]. On the other hand, the presence of pores smaller than 50 μm was observed in all the studied scaffolds. This kind of pores favors the function of metabolite transport and cell signaling. Pore sizes between 50 and 100 μm are important for cell adhesion. Pores with a diameter between 100 and 150 μm and larger than 200 μm were also observed. These pores are directly related to the formation of the osteonal unit and the biomineralization processes [23].

3.2. Compression test

The data of the compression modulus and maximum strength of the scaffolds are shown in Table 2. PCL/Ch/EPM scaffold showed better performance (greatest improvement in the compressive tests) than PCL/Ch scaffolds without extrapalleal protein from *Mytilus Californiensis* and PCL/Ch/EPI samples, which were functionalized with different methodology. Being 1.323 and 3.114, 1.077 and 2.46, and 0.42 and 1.46 MPa for compression modulus and maximum strength for PCL/Ch/EPM, PCL/Ch/EPI, and PCL/Ch scaffolds, respectively. In recent years, it has been proven that bone strength depends on its mass, geometry, structural properties, mineralization, and composition of the matrix, being called bone quality. Therefore, their mechanical properties are determined by the properties of mineralization, the composition of the matrix, and architecture. In consequence, any change in these will be related to their mechanical properties [9]. Therefore, reproducing the functional properties of natural bone in scaffolds requires the consideration of mechanical properties. The ideal scaffold (as already mentioned) should pose specific architectural, physicochemical, biological, and mechanical properties. In this work, the scaffolds have a natural and synthetic polymer in their composition, natural polymers have good biocompatibility, higher degradation rates, low immunogenicity, easy absorption, ability to inhibit the immune reaction, and induce immune tolerance, however, they have poor mechanical properties and difficulty in being controlled. Therefore, the use of a synthetic polymer and the protein optimized the mechanical properties of the scaffolds; this may be related to the inclusion of PCL and the protein during synthesis of the scaffolds that slowed down their degradation. Since PCL has slow degradation and functional groups of the protein interact with the polymer matrix forming intermolecular interactions, decreasing in pore size, and hence improved mechanical properties, a similar phenomenon was observed in previous studies [14,24].

Table 2. Maximum strength, deformation in maximum strength, and compression modulus of the PCL/Ch, PCL/Ch/EPI, and PCL/Ch/EPM scaffolds.

Sample	Maximum strength (MPa)	Deformation at maximum strength (mm)	Compression modulus (MPa)
PCL/Ch/EPM	3.1148 ± 0.08	1.3717 ± 0.001	1.3230 ± 0.032
PCL/Ch	2.4696 ± 0.14	1.0120 ± 0.012	1.0770 ± 0.024
PCL/Ch/EPI	1.4689 ± 0.23	0.9216 ± 0.13	0.4285 ± 0.010

3.3. Degradation analysis

The hydrolytic and enzymatic degradation of the PCL/Ch, PCL/Ch /EPI, and PCL/ Ch/EPM scaffolds were investigated by monitoring the weight loss during the degradation process (Figure 3). Chitosan biomaterials are mainly degraded by the action of lysozymes. The rapid degradation rates of chitosan scaffolds often limit their use *in vivo* systems.

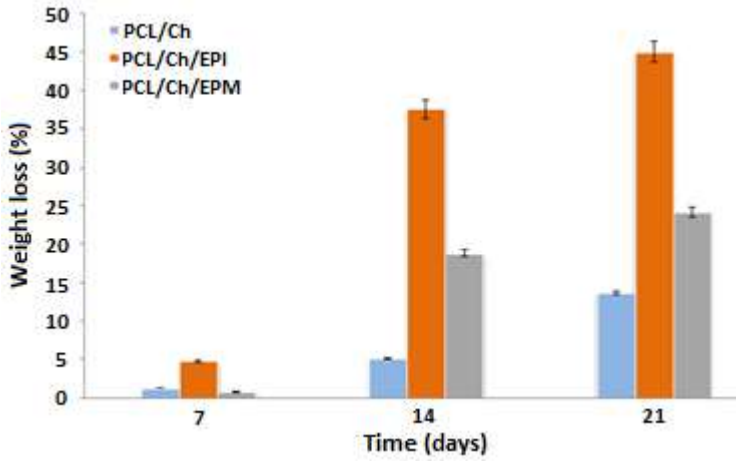

Figure 3. Hydrolytic and enzymatic degradation of the PCL/Ch, PCL/Ch /EPI, and PCL/ Ch/EPM.

The addition of other polymers, like polycaprolactone to the chitosan matrix, may influence the degradation kinetics, as seen on the PCL/Ch scaffold. This is because polycaprolactones are characterized by a slower degradation due to the semi-crystalline nature of PCL which hindrance water diffusion and thus decreases the hydrolytic degradation rate [25]. Other researchers have reported that the enzyme lysozyme degrades Chitosan/polycaprolactone materials in a period of 21 d [26]. After two weeks, significant percentage weight loss differences between the composite scaffolds were observed. At the end of the study, degradation of 13.69 ± 1.03% was observed for PCL/Ch, 45.02 ± 6.55% for PCL/Ch/EPI, and 24.17 ± 4.06% for PCL/Ch/EPM. It was found that both the protein presence and its addition methodology have a large effect on material degradation. When the protein is added by adsorption to the polymeric matrix surface (PCL/Ch /EPI), the degradation rate is larger than in the case where the protein is embedded in the polymeric matrix. This is because the protein in the PCL/Ch/EPM scaffold is part of the polymeric matrix, causing the degradation to be slower, major mechanical properties, and minor average pore compared to the PCL/Ch/EPI scaffold.

3.4. Bioactivity in vitro property

All the scaffolds, after being incubated in SBF for 3 weeks, were analyzed by FTIR, XRD and SEM-EDS. The infrared spectra of the PCL/Ch, PCL/Ch/EPI, and PCL/Ch/EPM scaffolds are shown in Figure 4. In these spectra, the absorption bands are observed at 1738 cm^{-1} corresponding to the carbonyl group (C = O), at 1336 cm^{-1} for the OH group, at 1228 cm^{-1} for the NH group, and 1216 cm^{-1} for the CO group. Various bands between 997 and 1154 cm^{-1} were also observed, and they are related to the bending vibration of the PO_4^{3-} groups. Inorganic carbonates (CO_3^{2-}) are seen at intervals of 832 to 880 and 1435 to 1496 cm^{-1} [23].

SEM images (Figure 4b) of the SBF tests revealed deposits of hydroxyapatite on the surface of the scaffolds with its characteristic cauliflower structure.

Figure 4c shows the diffractograms of the PCL/Ch, PCL/Ch/EPI, and PCL/Ch/EPM scaffolds where the polymeric matrices' main peaks are found at 2θ angles of 19.62° and 21.22° characteristic of the Ch and PCL, respectively. These polymeric scaffolds were exposed to the SBF solution for different periods (1, 2, and 3 weeks). After one week of exposure, the diffractograms of the PCL/Ch/EPI and PCL/Ch/EPM scaffolds show signals at 2θ angles of 25.8° and 31.7°, which are the most intense peaks of the hydroxyapatite phase. After three weeks new peaks appear at 46.7 and 75.3° (related to the hydroxyapatite phase) and peaks at 66° and 57° which are attributed to the amorphous calcium for $CaCO_3$ [27]. The bioactivity *in vitro* analysis suggests the formation of carbonate hydroxyapatite by the possible substitution of groups CO_3^{2-} by groups PO_4^{3-}. Therefore, it is expected to find crystalline phases and a Ca/P molar ratio related to the presence of apatite. The Ca/P molar ratio of the scaffolds obtained by EDS analyses is shown in Figure 4d. The Ca/P molar ratios were 1.69 and 1.56 for the PCL/Ch/EPI and PCL/Ch/EPM, respectively. These molar ratio values are promising since they are close to 1.68, the molar ratio that is related to the densification of hydroxyapatite. The PCL/Ch scaffolds show a Ca/P molar ratio of 3.12 making evident that the inclusion of protein improves the chitosan bioactivity and showing a hydroxyapatite layer with similar characteristics to the cortical bone in terms of carbonate content and Ca/P molar ratio [28]. This coating was formed on the scaffolds after 7 d, observing an increase with time. However, PCL/Ch/EPM scaffolds showed larger deposits of hydroxyapatite on their surface during the entire study period. Functional groups of PCL and chitosan ($-OH^-$ and $-NH_2^{+2}$), in addition to the −COOH functional groups of the protein (more polar than functional groups of polymeric matrices) in conjunction with the ions present in SBF stimulates more hydroxyapatite formation. This agrees with other investigations, in which they have had to carry out a surface treatment to accelerate the nucleation and growth of hydroxyapatite crystals [29]. The peaks in the PCL/Ch scaffold diffractogram at 2θ angles of 57°, 66°, and 75° are observed after the third week of exposure to SBF and suggest the presence of hydroxyapatite phase precursors and carbonated hydroxyapatite. The intensity of the peaks of the PCL/Ch/EPM diffractogram shows higher intensities than the peaks of the PCL/Ch/EPI diffractograms throughout the study. These results suggest that the nucleation and growth of apatite crystals were less favored in the scaffolds functionalized by immersion. This can be attributed to the fact that the protein in PCL/Ch/EPM scaffolds is homogeneously distributed on its surface and the exposure of functional groups such as −COOH responsible for the coordination of Ca^{2+} or the protein are released according to the degradation polymeric matrix. While the

PCL/Ch/EPI scaffold releases the protein, more quickly allowing the formation of oligomers since at higher protein concentration increased the tendency to aggregate [30]. Additionally, increasing the number of reactive groups in the scaffolds would enhance the formation of bone-like apatite with a Ca/P ratio of 1.6 close to the human bone as seen in both extrapalleal fluid protein scaffolds [31].

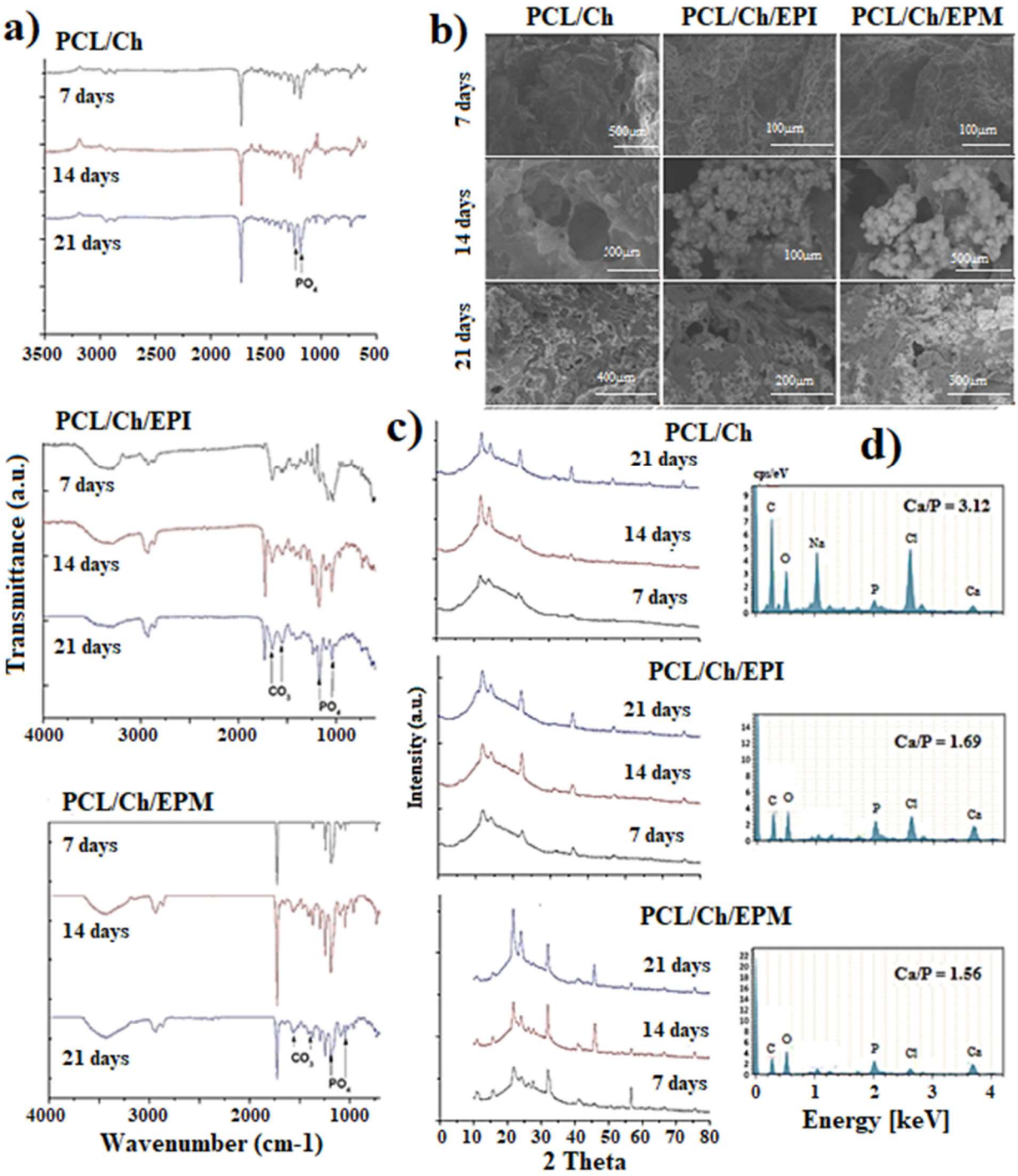

Figure 4. (a) Infrared spectra, (b) SEM images, (c) diffractograms, and EDS analyses of PCL/Ch, PCL/Ch/EPI, and PCL/Ch/EPM scaffolds at 7, 14, and 21 d after being exposed to SBF.

3.5. Cell adhesion, cell differentiation, and cytocompatibility

The adhesion and proliferation of osteoblasts were determined on PCL/Ch, PCL/Ch/EPI, and PCL/Ch/EPM scaffolds to infer their ability to assist tissue regeneration *in vivo*. The results of the evaluation cell population using MTT assay and fluorescent staining are shown in Figure 5. Figure 5b represents the confocal microscopic images showing osteoblasts' adhesion and growth on the surface of the 3 scaffolds and control after 7 d of cell culture. In Figure 5b, protein incorporation interestingly improved the spreading and proliferation of cells with characteristic morphology and integration in the PCL/Ch/EPI and PCL/Ch/EPM after 7 d of osteoblast seeded on the surface of the scaffolds. It is a direct indication of the better cell-to-cell interaction of the cells to the polymer matrix, confirming what was obtained by the MTT analysis (Figure 5a).

Figure 5c shows the results of the alkaline phosphatase activity of the osteoblasts seeded in the scaffolds. As alkaline phosphatase activity is indicative of osteoblast activity and the initial stage of osteoblast differentiation, these results suggest that PCL/Ch/EPI and PCL/Ch/EPM scaffolds may promote osteoblast differentiation earlier than the PCL/Ch scaffold. The PCL/Ch/EPM scaffold was found to be superior, as observed in the cell viability and cell adhesion.

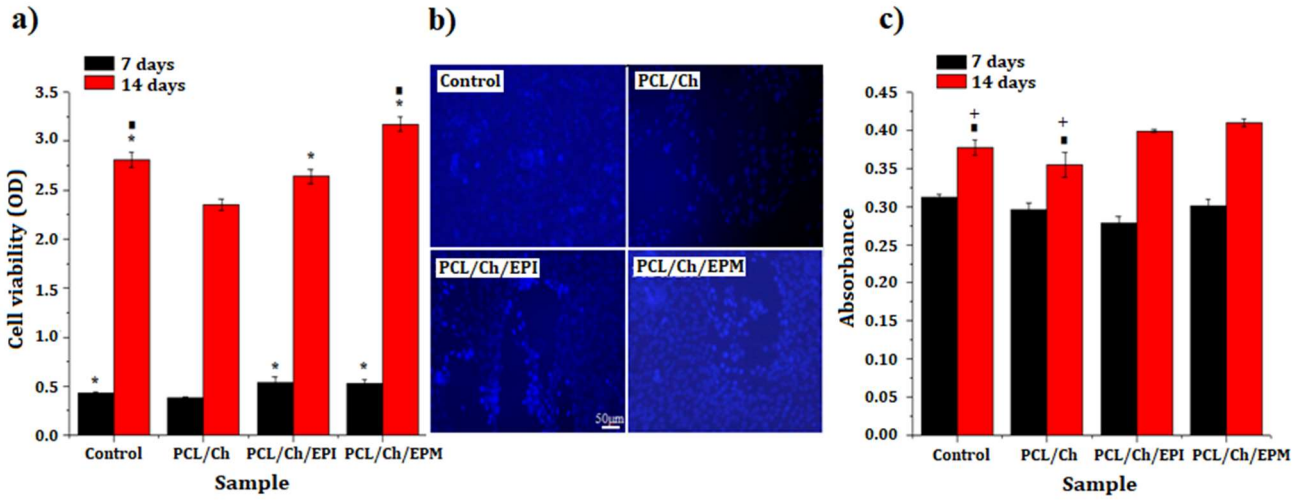

Figure 5. (a) Evaluation of the cell viability through MTT assay, from 7 and 14 d. (b) Observation of the osteoblasts seeded in the materials, through fluorescent staining (DAPI and Calcein AM). (c) Analysis of the bioactivity of the materials through alkaline phosphatase enzyme at 7 and 14 d.

Cell adhesion is optimal on moderately hydrophilic surfaces that favor the adsorption of proteins involved in cell adhesion in their native conformation and accessible recognition sequences. In addition, it has been observed that the surrounding proteins in the extracellular matrix interact to regulate cell development (proliferation, differentiation, migration, and adhesion within the material). Other studies carried out with protein extracted from the *Mytilus* family, showed that the water-soluble protein of *Mytilus edulis* showed a high osteogenic activity [32], and more recently with the

peptide (PME-1) identified from the *Mytilus edulis* proteins it promotes proliferation and differentiation of osteoblasts [33]. Protein-functionalized supports have already been reported to be responsible for transporting and controlling growth factors [34]. The proliferation behavior can be attributed to the protein present in these materials that share amino groups with the polymer matrix. Many metabolic and cell cycle processes have been attributed to the diversity of amino groups in the interstitial space of cells. These processes include cell proliferation, nucleic acid packaging, modulation of membrane receptors, modulation of ion channels, and regulation of gene expression [35].

As observed in the investigation by Jaramillo et al., *Mytilus californiensis* protein facilitates the apatite nucleation on the chitosan scaffold surface during the *in vitro* biomineralization process [17]. Other research has shown that the proteins obtained from the *Mytilus* family have helped the formation of crystals during an *in vitro* biomineralization process, as soluble matrix extracts of *Mytilus edulis* [36], and protein hydrolysates of *Mytilus edulis* [37].

4. Conclusion

PCL/Ch scaffolds functionalized with protein of *Mytilus californiensis* promote apatite formation, whereas the presence of EP in the scaffolds increases the mechanical properties, accelerates the degradation of the material, promotes osteoblast differentiation, and favors osteoblast adhesion and proliferation. The integration of the protein to the polymeric matrix during the synthesis of the material (PCL/Ch/EPM) allowed obtaining scaffold with higher mechanical properties compared to the material that was immersed in the protein solution (PCL/Ch/EPI). On the other hand, the PCL/Ch/EPM and PCL/Ch/EPI scaffolds showed a higher speed in their enzymatic hydrolytic biodegradation process compared to the PCL/Ch scaffolds. However, among the PCL/Ch/EPM and PCL/Ch/EPI scaffolds, the second was the one that showed the greatest weight loss during the study periods, finding that the EP protein integration methodology allows the control of the biodegradation process of the scaffolds. Furthermore, the PCL/Ch/EPM scaffold showed greater bioactivity and cell proliferation than the PCL/Ch/EPI and PCL/Ch scaffold, without noticeable morphological alterations in the cellular structures that denote harmful effects. These results suggest that PCL/Ch scaffolds with EP are novel and attractive for the bone regeneration area.

Conflict of interest

The authors have no conflict of interest with the publication of this article.

References

1. Su X, Wang T, Guo S (2021) Applications of 3D printed bone tissue engineering scaffolds in the stem cell field. *Regen Ther* 16: 63–72. https://doi.org/10.1016/j.reth.2021.01.007
2. Safari B, Aghanejad A, Roshangar L, et al. (2020) Osteogenic effects of the bioactive small molecules and minerals in the scaffold-based bone tissue engineering. *Colloid Surface B* 198: 111462. https://doi.org/10.1016/j.colsurfb.2020.111462

3. Xia P, Zhang K, Yan S, et al. (2021) Biomimetic, biodegradable, and osteoinductive Microgels with open porous structure and excellent injectability for construction of microtissues for bone tissue engineering. *Chem Eng J* 414: 128714. https://doi.org/10.1016/j.cej.2021.128714
4. Prasad A (2021) State of art review on bioabsorbable polymeric scaffolds for bone tissue engineering. *Mater Today Proc* 44: 1391–1400. https://doi.org/10.1016/j.matpr.2020.11.622
5. Ma C, Wang H, Chi Y, et al. (2021) Preparation of oriented collagen fiber scaffolds and its application in bone tissue engineering. *Appl Mater Today* 22: 100902. https://doi.org/10.1016/j.apmt.2020.100902
6. Park J, Lee SJ, Jung TG, et al. (2021) Surface modification of a three-dimensional polycaprolactone scaffold by polydopamine, biomineralization, and BMP-2 immobilization for potential bone tissue applications. *Colloids Surf B* 199: 111528. https://doi.org/10.1016/j.colsurfb.2020.111528
7. Kundu K, Afshar A, Katti DR, et al. (2020) Composite nanoclay-hydroxyapatite-polymer fiber scaffolds for bone tissue engineering manufactured using pressurized gyration. *Compos Sci Technol* 202: 108598. https://doi.org/10.1016/j.compscitech.2020.108598
8. Shaabani A, Sedghi R, Motasadizadeh H, et al. (2021) Self-healable conductive polyurethane with the body temperature-responsive shape memory for bone tissue engineering. *Chem Eng J* 411: 128449. https://doi.org/10.1016/j.cej.2021.128449
9. Wang L, Lu R, Hou J, et al. (2020) Application of injectable silk fibroin/graphene oxide hydrogel combined with bone marrow mesenchymal stem cells in bone tissue engineering. *Colloids Surf A* 604: 125318. https://doi.org/10.1016/j.colsurfa.2020.125318
10. Wuriantika MI, Utomo J, Nurhuda M, et al. (2021) Nanostructure, porosity and tensile strength of PVA/Hydroxyapatite composite nanofiber for bone tissue engineering. *Mater Today Proc* 44: 3203–3206. https://doi.org/10.1016/j.matpr.2020.11.438
11. Pandit A, Indurkar A, Deshpande C, et al. (2021) A systematic review of physical techniques for chitosan degradation. *Carbohydr Polym* 2: 100033. https://doi.org/10.1016/j.carpta.2021.100033
12. Madni A, Kousar R, Naeem N, et al. (2021) Recent advancements in applications of chitosan-based biomaterials for skin tissue engineering. *J Bioresour Bioprod* 6: 128714. https://doi.org/10.1016/j.jobab.2021.01.002
13. Li J, Zhuang S (2020) Antibacterial activity of chitosan and its derivatives and their interaction mechanism with bacteria: Current state and perspectives. *Eur Polym J* 138: 109984. https://doi.org/10.1016/j.eurpolymj.2020.109984
14. Bulbul YE, Uzunoglu T, Dilsiz N, et al. (2020) Investigation of nanomechanical and morphological properties of silane-modified halloysite clay nanotubes reinforced polycaprolactone bio-composite nanofibers by atomic force microscopy. *Polym Test* 92: 106877. https://doi.org/10.1016/j.polymertesting.2020.106877
15. Voniatis C, Barczikai D, Gyulai G, et al. (2021) Fabrication and characterisation of electrospun Polycaprolactone/Polysuccinimide composite meshes. *J Mol Liq* 323: 115094. https://doi.org/10.1016/j.molliq.2020.115094
16. Zhao YQ, Yang JH, Ding X, et al. (2020) Polycaprolactone/polysaccharide functional composites for low-temperature fused deposition modelling. *Bioact Mater* 5: 185–191. https://doi.org/10.1016/j.bioactmat.2020.02.006

17. Jaramillo-Martínez S, Vargas-Requena C, Rodríguez-Gónzalez C, et al. (2019) Effect of extrapallial protein of Mytilus californianus on the process of in vitro biomineralization of chitosan scaffolds. *Heliyon* 5: e02252. https://doi.org/10.1016/j.heliyon.2019.e02252
18. Urbanek O, Sajkiewicz P, Pierini F (2017) The effect of polarity in the electrospinning process on PCL/chitosan nanofibres' structure, properties and efficiency of surface modification. *Polymer* 124: 168–175. https://doi.org/10.1016/j.polymer.2017.07.064
19. Zhang C, Zhai T, Turng LS, et al. (2015) Morphological, mechanical, and crystallization behavior of polylactide/polycaprolactone blends compatibilized by L-lactide/caprolactone copolymer. *Ind Eng Chem Res* 54: 9505–9511. https://doi.org/10.1021/acs.iecr.5b02134
20. Sarasam A, Madihally SV (2005) Characterization of chitosan—polycaprolactone blends for tissue engineering applications. *Biomaterials* 26: 5500–5508. https://doi.org/10.1016/j.biomaterials.2005.01.071
21. Fabian H, Mäntele W (2006) Infrared spectroscopy of proteins, *Handbook of Vibrational Spectroscopy*, 1 Ed., New York: Wiley Online Library.
22. Fadaie M, Mirzaei E, Geramizadeh B, et al. (2018) Incorporation of nanofibrillated chitosan into electrospun PCL nanofibers makes scaffolds with enhanced mechanical and biological properties. *Carbohydr Polym* 199: 628–640. https://doi.org/10.1016/j.carbpol.2018.07.061
23. Martel-Estrada SA, Olivas-Armendáriz I, Santos-Rodríguez E, et al. (2014) Evaluation of in vitro bioactivity of Chitosan/Mimosa tenuiflora composites. *Mater Lett* 119: 146–149. https://doi.org/10.1016/j.matlet.2014.01.004
24. Wang F, Guo Y, Lv R, et al. (2020) Development of nano-tricalcium phosphate/polycaprolactone/platelet-rich plasma biocomposite for bone defect regeneration. *Arab J Chem* 13: 7160–7169. https://doi.org/10.1016/j.arabjc.2020.07.021
25. Bil M, Hipś I, Mrówka P, et al. (2020) Studies on enzymatic degradation of multifunctional composite consisting of chitosan microspheres and shape memory polyurethane matrix. *Polym Degrad Stab* 182: 109392. https://doi.org/10.1016/j.polymdegradstab.2020.109392
26. Houreh AB, Masaeli E, Nasr-Esfahani MH (2021) Chitosan/polycaprolactone multilayer hydrogel: A sustained Kartogenindelivery model for cartilage regeneration. *Int J Biol Macromol* 177: 589–600. https://doi.org/10.1016/j.ijbiomac.2021.02.122
27. Ureña J, Tsipas S, Jiménez-Morales A, et al. (2018) In-vitro study of the bioactivity and cytotoxicity response of Ti surfaces modified by Nb and Mo diffusion treatments. *Surf Coat Technol* 335: 148–158. https://doi.org/10.1016/j.surfcoat.2017.12.009
28. Choong CSN, Triffitt JT (2005) Improved bone cellular activity through the use of calcium phosphate coated polymeric scaffolds. *Bone* 36: S103–S479.
29. Bayrak GK, Demirtaş TT, Gümüşderelioğlu M (2012) Microwave-induced biomimetic approach for hydroxyapatite coatings of chitosan scaffolds. *Carbohydr Polym* 157: 803–813. https://doi.org/10.1016/j.carbpol.2016.10.016
30. Chavira GNJ (2012) Evaluación de la capacidad de la proteína del fluido extrapalial de Mytilus Edulis de coordinar calcio [Dissertation]. Autonomous University of Ciudad Juárez (In Mexico).
31. Saravanan S, Leena RS, Selvamurugan N (2016) Chitosan based biocomposite scaffolds for bone tissue engineering. *Int J Biol Macromol* 93: 1354–1365. https://doi.org/10.1016/j.ijbiomac.2016.01.112

32. Xu Z, Zhao F, Chen H, et al. (2019) Nutritional properties and osteogenic activity of enzymatic hydrolysates of proteins from the blue mussel (Mytilus edulis). *Food Funct* 10: 7745–7754. https://doi.org/10.1039/C9FO01656B
33. Xu Z, Fan F, Chen H, et al. (2021) Absorption and transport of a Mytilus edulis-derived peptide with the function of preventing osteoporosis. *Food Funct* 12: 2102–2111. https://doi.org/10.1039/D0FO02353A
34. He B, Zhao J, Ou Y, et al. (2018) Biofunctionalized peptide nanofiber-based composite scaffolds for bone regeneration. *Mat Sci Eng C* 90: 728–738. https://doi.org/10.1016/j.msec.2018.04.063
35. Guasco Herrera C, Chávez Servín JL, Ferriz Martínez RA, et al. (2014) Poliaminas: pequeños gigantes de la regulación metabólica. *REB* 33: 51–57.
36. Roque J, Molera J, Vendrell-Saz M, et al. (2004) Crystal size distributions of induced calcium carbonate crystals in polyaspartic acid and Mytilus edulis acidic organic proteins aqueous solutions. *J Cryst Growth* 262: 543–553. https://doi.org/10.1016/j.jcrysgro.2003.10.052
37. Hyung JH, Ahn CB, Je JY (2018) Blue mussel (Mytilus edulis) protein hydrolysate promotes mouse mesenchymal stem cell differentiation into osteoblasts through up-regulation of bone morphogenetic protein. *Food Chem* 242: 156–161. https://doi.org/10.1016/j.foodchem.2017.09.043

AIMS Press